AD-A038 267 ILLINOIS UNIV AT URBANA-CHAMPAIGN COORDINATED SCIENCE LAB F/G 20/5
TWO DIMENSIONAL ANALYSIS OF THE GAAS DOUBLE HETFRO STRIPE-GEOME--ETC(U)
DEC 76 L GRUN DAAB07-72-C-0259
UNCLASSIFIED R-750 NL

1 OF 1
AD A038267

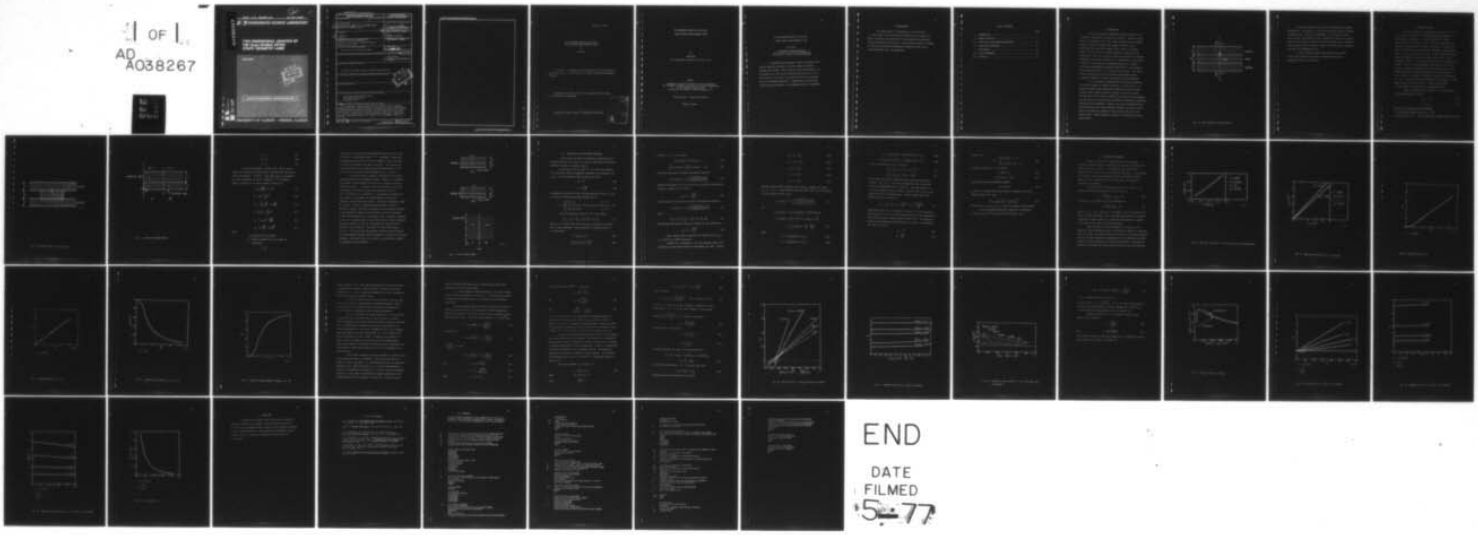

END

DATE FILMED
5-77

AD A038267

(12) FC.

REPORT R-750 DECEMBER, 1976 UILU-ENG 76-2238

CSL COORDINATED SCIENCE LABORATORY

TWO DIMENSIONAL ANALYSIS OF THE GaAs DOUBLE HETRO STRIPE-GEOMETRY LASER

LEON GRUN

DDC RECEIVED APR 15 1977 C

APPROVED FOR PUBLIC RELEASE. DISTRIBUTION UNLIMITED.

AD No. DDC FILE COPY

UNIVERSITY OF ILLINOIS – URBANA, ILLINOIS

UNCLASSIFIED

SECURITY CLASSIFICATION OF THIS PAGE (When Data Entered)

REPORT DOCUMENTATION PAGE

READ INSTRUCTIONS BEFORE COMPLETING FORM

1. REPORT NUMBER

2. GOVT ACCESSION NO.

3. RECIPIENT'S CATALOG NUMBER

4. TITLE (and Subtitle)

TWO DIMENSIONAL ANALYSIS OF THE GaAs DOUBLE HETERO STRIPE-GEOMETRY LASER,

5. TYPE OF REPORT & PERIOD COVERED

Technical Report,

6. PERFORMING ORG. REPORT NUMBER

R-750 , UILU-ENG-76-2238

7. AUTHOR(s)

Leon Grun

8. CONTRACT OR GRANT NUMBER(s)

DAAB07-72-C-0259

9. PERFORMING ORGANIZATION NAME AND ADDRESS

Coordinated Science Laboratory
University of Illinois at Urbana-Champaign
Urbana, Illinois 61801

10. PROGRAM ELEMENT, PROJECT, TASK AREA & WORK UNIT NUMBERS

11. CONTROLLING OFFICE NAME AND ADDRESS

Joint Services Electronics Program

12. REPORT DATE

Dec[redacted] 1976

13. NUMBER OF PAGES

40

14. MONITORING AGENCY NAME & ADDRESS(if different from Controlling Office)

15. SECURITY CLASS. (of this report)

UNCLASSIFIED

15a. DECLASSIFICATION/DOWNGRADING SCHEDULE

16. DISTRIBUTION STATEMENT (of this Report)

Approved for public release; distribution unlimited.

17. DISTRIBUTION STATEMENT (of the abstract entered in Block 20, if different from Report)

DDC
RECEIVED
APR 15 1977
C

18. SUPPLEMENTARY NOTES

19. KEY WORDS (Continue on reverse side if necessary and identify by block number)

GaAs Double Petero Stripe Laser
Two Dimensional Anslysis
Fundamental Mode

20. ABSTRACT (Continue on reverse side if necessary and identify by block number)

The GaAlAs/GaAs stripe-geometry laser is analyzed using a recently developed technique called the effective dielectric constant (EDC) method. Unlike previously reported techniques, the EDC method allows both vertical and horizontal directions in the cross section of the laser to be taken into account in analyzing the field confinement mechanism. Computed data on field concentration and cutoff behavior of the fundamental mode are present

DD FORM 1 JAN 73 1473 EDITION OF 1 NOV 65 IS OBSOLETE

UNCLASSIFIED 097700

SECURITY CLASSIFICATION OF THIS PAGE (When Data Entered)

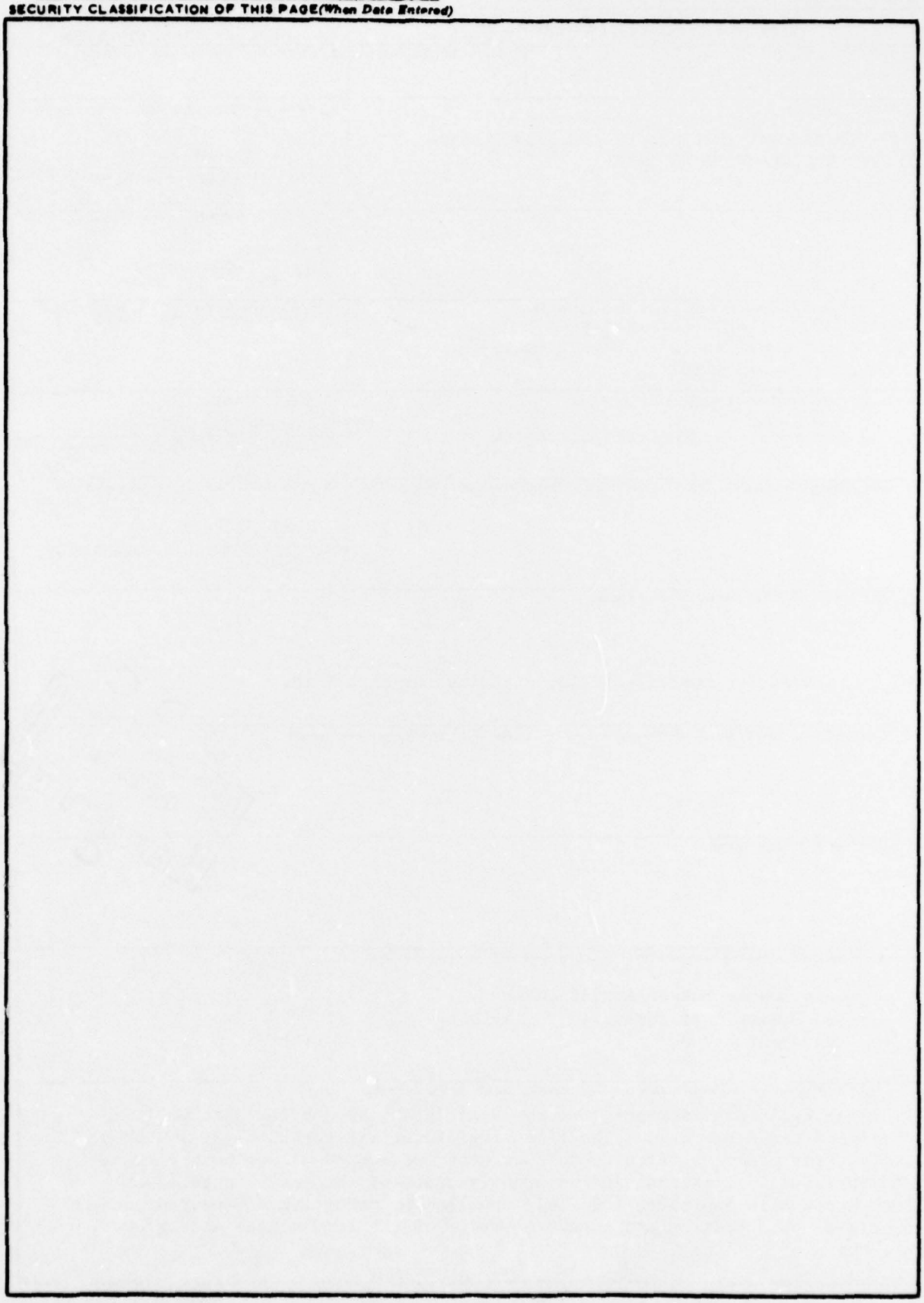

UILU-ENG 76-2238

TWO DIMENSIONAL ANALYSIS OF THE GaAs DOUBLE HETERO STRIPE-GEOMETRY LASER

by

Leon Grun

This work was supported in part by the Joint Services Electronics Program (U.S. Army, U.S. Navy and U.S. Air Force) under Contract DAAB-07-72-C-0259.

Reproduction in whole or in part is permitted for any purpose of the United States Government.

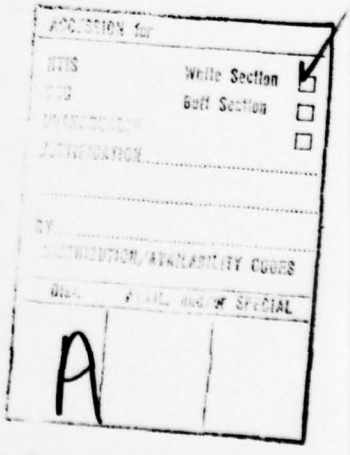

Approved for public release. Distribution unlimited.

TWO DIMENSIONAL ANALYSIS OF THE GaAs DOUBLE HETERO STRIPE-GEOMETRY LASER

BY

LEON GRUN

B.S. Polytechnic Institute of New York, 1975

THESIS

Submitted in partial fulfillment of the requirements
for the degree of Master of Science of Electrical Engineering
in the Graduate College of the
University of Illinois at Urbana-Champaign, 1977

Thesis Advisor: Professor Raj Mittra

Urbana, Illinois

TWO DIMENSIONAL ANALYSIS OF THE GaAs DOUBLE HETERO STRIPE-GEOMETRY LASER

Leon Grun

Coordinated Science Laboratory
and Department of Electrical Engineering
University of Illinois at Urbana-Champaign

The GaAℓAs/GaAs stripe-geometry laser is analyzed using a recently developed technique called the effective dielectric constant (EDC) method. Unlike previously reported techniques, the EDC method allows both vertical and horizontal directions in the cross section of the laser to be taken into account in analyzing the field confinement mechanism. Computed data on field concentration and cutoff behavior of the fundamental mode are presented.

ACKNOWLEDGEMENT

The author wishes to acknowledge Dr. Tatsuo Itoh and Dr. Tullio Rozzi, who contributed the theoretical work on which this thesis is based on, and thank them for their great help and patience during the course of this research. Also my special thanks to Professor Raj Mittra who guided and encouraged me through my studies and to Trudy Williams who typed this manuscript.

TABLE OF CONTENTS

I. INTRODUCTION

Double-hetero-junction GaAℓAs/GaAs lasers constitute a key component in integrated and fiber optical systems. The basic configuration is illustrated in Fig. (1a). When a strong dc bias is applied between the stripe electrodes, the segment of the GaAs layer immediately below the stripe becomes active, resulting in lasing action. The GaAs layer has a higher dielectric constant than the GaAℓAs layer. Hence, it is easy to explain the existence of a guiding mechanism in the vertical direction (i.e. perpendicular to the layers), by means of a conventional slab waveguide analysis [2]. However, it has been experimentally observed that the field is also confined in the transverse direction (i.e., parallel to the layers). This effect cannot be explained in terms of an infinite slab waveguide since no physical mechanism is present for transverse field confinement.

It is now generally accepted that the dielectric properties of the active region are slightly altered by the lasing action. It has been assumed by some workers that lasing action causes a slight increase of the relative dielectric constant in the active region (of the order of 10^{-3}), which is sufficient to explain field confinement. Only the real part of the dielectric constant was considered in explaining transverse field confinement. However, some recent investigations [3], indicate the real part of the dielectric constant in the active region need not be higher and, indeed, may even be lower than that in the passive region. Modal confinement is shown to be possible by the gain action itself.

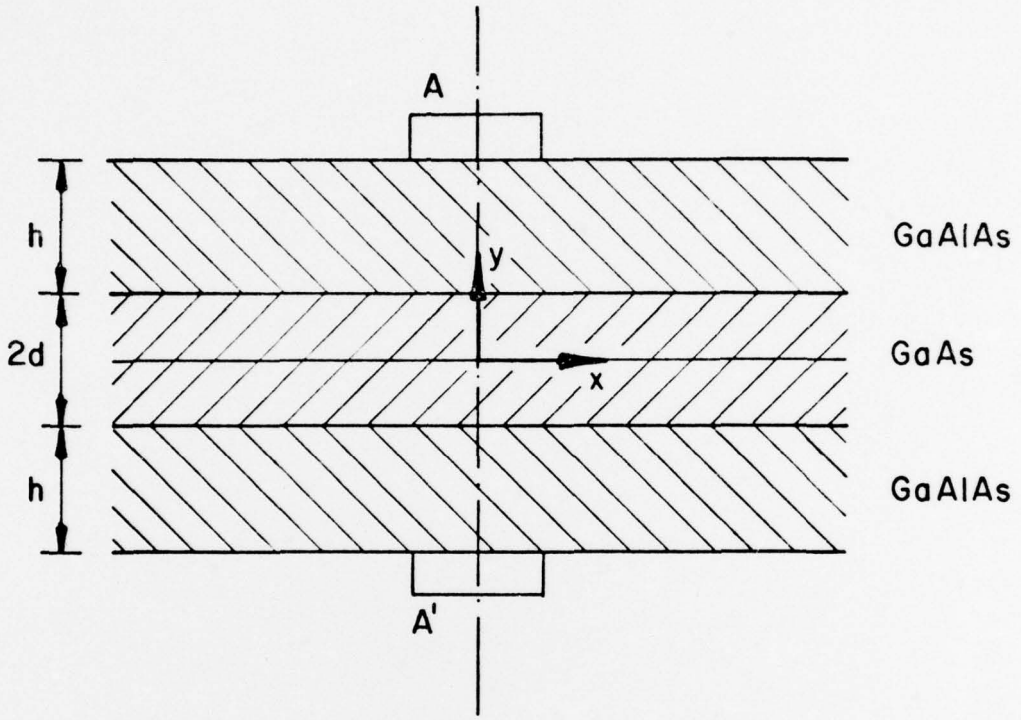

Fig. 1a: Basic Geometry of the GaAs laser.

In previous analysis [3], the x and y directions were treated independently. For instance, in [3], only the structure which is infinite in extent in the y direction is considered. In the analysis in this paper, however, the finiteness in the y direction is taken into account by the use of the concept of effective dielectric constants (EDC), which has been successfully used to analyze a number of lossless passive dielectric waveguides and components [4], [5].

In the following sections we will describe the analysis of the laser structure and a number of numerical data for the fundamental mode will be presented.

II. METHOD OF ANALYSIS

The basic geometry of the GaAs laser is shown in Fig. (1a). A GaAs layer of thickness 2d is sandwiched between two identical GaAlAs layers of thickness h. When an appropriate d.c bias is applied between the electrodes A and A', the GaAs region under the electrodes becomes active and causes a laser action. We model this effect by assigning the region under the electrode a complex permittivity $\epsilon_1' + j\epsilon_1''$, as shown in Fig. (1b). In this figure the presence of the electrodes is ignored as its effect on the optical field is negligible. From Fig. (1a) we observe that the field is symmetric with respect to the y axis and antisymmetric with respect to the x axis. Therefore a magnetic and electric wall can be placed in the y and x planes, respectively, without changing the field configurations. It is, hence, only necessary to consider the quadrant illustrated in Fig. (2). Along the x direction we distinguish two regions: I. which contains the active material and II, which is purely passive. For the present, all dielectrics are considered lossless.

Region I contains three dielectrics: (1) the active GaAs with complex dielectric constant

$$\epsilon_1 = \epsilon_1' + j\epsilon_1'' \tag{1a}$$

$$0 < \epsilon_1'' \ll \epsilon_1' \tag{1b}$$

where $\epsilon_1'' > 0$ represents the gain mechamism.

(2) the lossless GaAlAs with real $\epsilon_2 > 0$ and

(3) the air with $\epsilon_3 = 1$. Also we assume the following relations to hold:

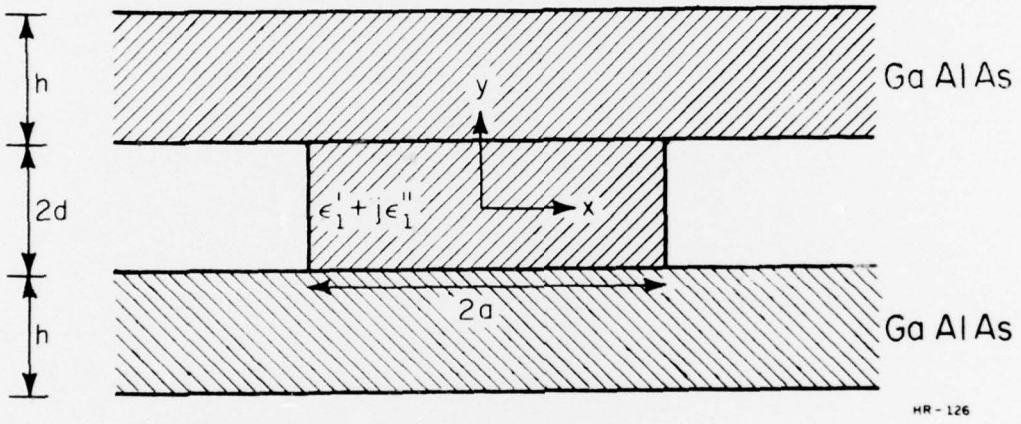

Fig. 1b: Waveguide model of the GaAs laser.

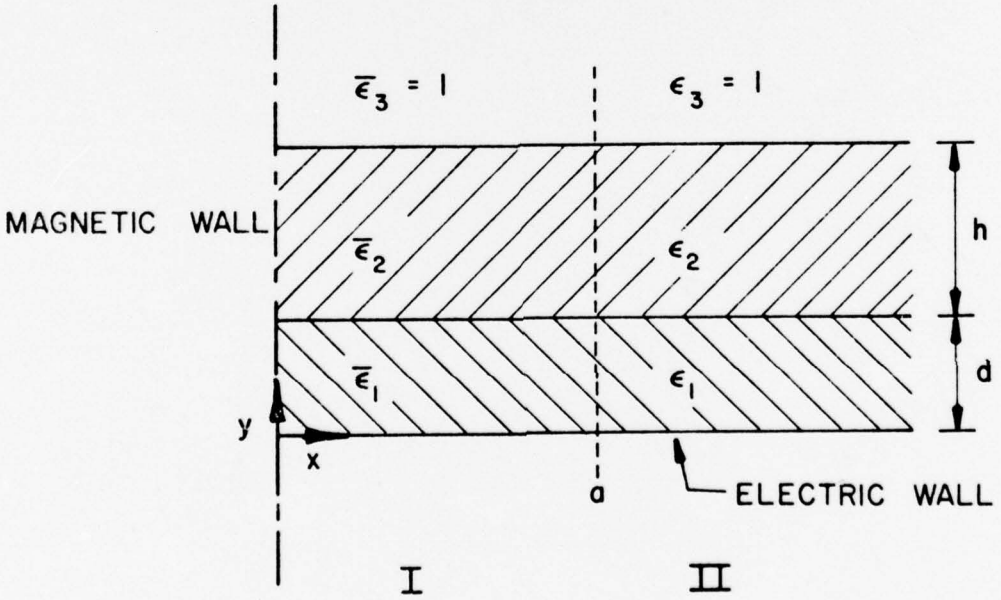
$\bar{\epsilon}_3 = 1$
$\epsilon_3 = 1$
MAGNETIC WALL
$\bar{\epsilon}_2$
ϵ_2
h
$\bar{\epsilon}_1$
ϵ_1
d
y
x
a
ELECTRIC WALL
I
II

$$\bar{\epsilon}_2 \approx \epsilon_2 \tag{2a}$$

$$\epsilon_1' > \bar{\epsilon}_2 \tag{2b}$$

$$\epsilon_1 > \epsilon_2 \tag{2c}$$

A dielectric waveguide, as shown in Fig. (1b) is known to support the propagation of hybrid modes, classified into two possible field configurations: E^x and E^Y. These modes can be represented by two scalar potentials, ϕ^e and ϕ^H. Assuming a $e^{-jk_z z}$ dependence, Maxwells equations [1] in terms of these potentials are:

$$E_x = \frac{1}{\epsilon_r} \frac{\partial^2 \phi^e}{\partial y \partial x} + \omega\mu\, k_z \phi^H \tag{3a}$$

$$H_y = (k_z^2 - \frac{\partial^2}{\partial x^2})\phi^H \tag{3b}$$

$$E_z = - \frac{jk_z}{\epsilon_r} \frac{\partial \phi^e}{\partial y} - j\omega\mu \frac{\partial \phi^H}{\partial x} \tag{3c}$$

$$E_y = \frac{1}{\epsilon_r} (k_z^2 - \frac{\partial^2}{\partial x^2})\phi^e \tag{4a}$$

$$H_x = - \omega\epsilon_o k_z \phi^e + \frac{\partial^2 \phi^H}{\partial y \partial x} \tag{4b}$$

$$H_z = j\omega\epsilon_o \frac{\partial \phi^e}{\partial x} - jk_z \frac{\partial \phi^H}{\partial Y} \tag{4c}$$

where

ϵ_o = permittivity of free space

ϵ_r = relative permittivity in the region of application

$$j = \sqrt{-1}$$

However, due to the excitation the dominant electric field is in the y direction. We therefore assume $\phi^H = 0$. Furthermore, because the differences between $\bar{\epsilon}_1$ and ϵ_1 as well as between $\bar{\epsilon}_1$ and ϵ_2 are small, we assume the transverse wave numbers are small. This implies that second derivatives can be neglected and the dominant mode is of the E^y type with the principal field components E_y, H_x, H_z and E_z.

A rigorous solution of Maxwell's equations for the present laser geometry would be exceedingly complex. However, it is possible to introduce a simplification by the use of the concept of effective dielectric constant. If regions I and II were infinitely wide, they would reduce to the double layered slab structures as shown in Fig. (3a) and Fig. (3b), respectively. The propagation constants for these double slab waveguides can be determined by matching the tangential fields across each boundary. Both these structures can then be replaced by infinite, homogeneous regions having a effective dielectric constant, which may be thought of as the dielectric constant of the hypothetical medium in which the phase velocity is identical to that of the surface wave in the original (slab) structure. Referring to Fig. (2), we replace region I and II with vertical slabs of effective dielectric constant ϵ_{e1} and ϵ_{e2}, even though these regions are not infinite in the x direction. The result is the structure shown in Fig. (3c). We can now solve the eigenvalue equation of this structure for the propagation constant, which is assumed to be that of the original structure. Notice that since $\bar{\epsilon}_1$ is complex, ϵ_{e1} must also be complex to represent the gain mechanism.

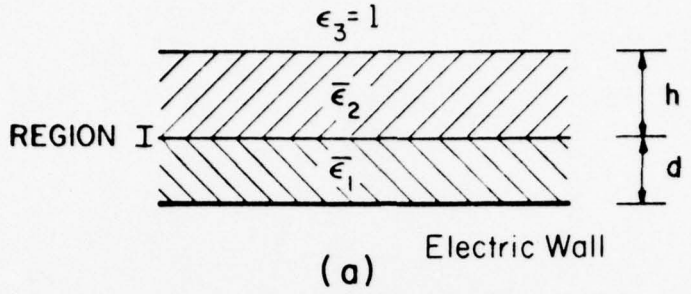

(a)

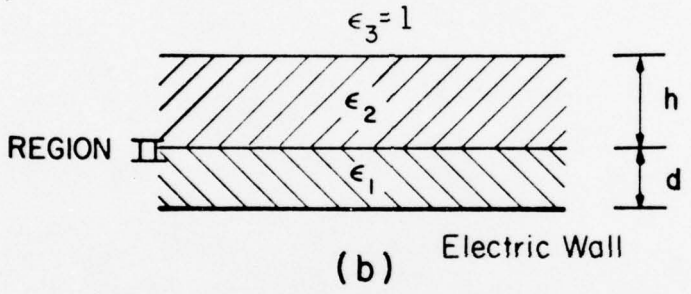

(b)

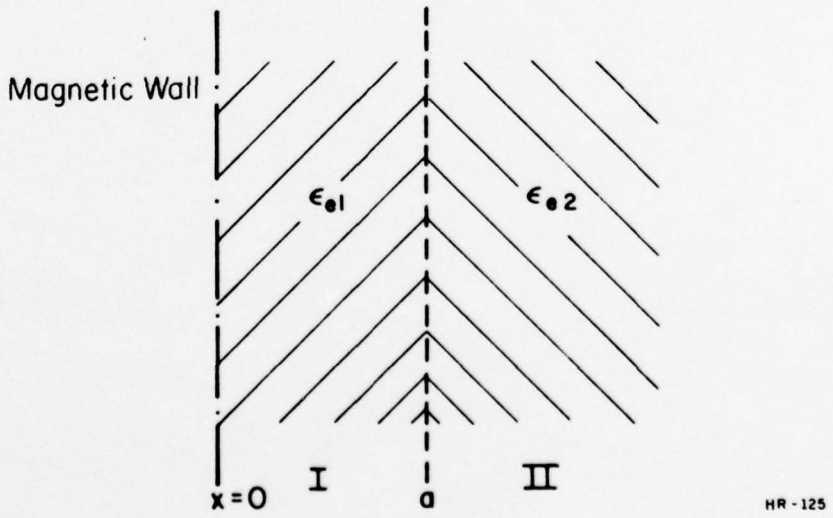

(c)

Fig. 3: Slab structure model.

III. DERIVATION OF THE EIGENVALUE EQUATIONS

In this section we derive the eigenvalue equations for the structures shown in Fig. (3a), (3b), and (3c) and define the effective dielectric constant for regions I and II.

Noting that for the E^Y mode, $\phi^H = 0$, we see from equations (3a) through (4c) that the tangential components to be matched are H_x and E_z. The relationships between H_x and E_z and ϕ^e are

$$H_x \sim \phi^e \tag{5a}$$

$$E_z \sim \frac{1}{\epsilon_r} \frac{\partial \phi^e}{\partial y} \tag{5b}$$

Considering the structure in Fig. (3b) and noting that since $E_z = 0$ at $y = 0$, we can choose the following function for ϕ^e.

$$\phi^e = \begin{cases} A \cos k_{y2} y & d > y > 0 \\ B^c \cos h\,(\eta_2 (y-d)) + B^s \sin h\,(\eta_2 (y-d)) & d+h < y < d \\ C \exp[-\xi_2 (y-d-h)] & y > d + h \end{cases} \tag{6}$$

Since the fields must match for all z we also have,

$$k_{z2}^2 = \epsilon_1 k_o^2 - k_{y2}^2 = \epsilon_2 k_o^2 + \eta_2^2 = k_o^2 + \xi_2^2 \tag{7}$$

where ξ_2 is real and greater than zero, k_{y2} is real and η_2 is purely real or purely imaginary. Using equation (6) we match H_x and E_z at $y = d$ and obtain

$$A \cos k_{y2} d = B^c \tag{8a}$$

$$-\frac{A}{\epsilon_1} k_{y2} \sin k_{y2} d = \frac{\eta_2}{\epsilon_2} B^s \tag{8b}$$

Similarly at $y = d + h$ we obtain

$$B^c \cosh(\eta_2 h) + B^s \sinh(\eta_2 h) = C \tag{9a}$$

$$\frac{\eta_2}{\epsilon_2} B^c \sinh(\eta_2 h) + \frac{\eta_2}{\epsilon_2} B^s \cosh(\eta_2 h) = -\xi_2 C \tag{9b}$$

After some manipulation we obtain the eigenvalue equation

$$k_{y2} \tan k_{y2} d = \eta_2 \frac{\epsilon_1}{\epsilon_2} \frac{\eta_2 \tanh(\eta_2 h) + \epsilon_2 \xi_2}{\epsilon_2 \xi_1 \tanh(\eta_2 h) + \eta_2} \tag{10}$$

Together with equation (7) we can solve for k_{y2} and define the effective dielectric constant for Fig. (3b) as

$$\epsilon_{e2} = \epsilon_1 - \left(\frac{k_{y2}}{k_o}\right)^2 \tag{11}$$

A similar analysis for Figure (3a) leads to the eigenvalue equation

$$k_{y1} \tan k_{y1} d = \eta_1 \frac{\epsilon_1}{\epsilon_2} \frac{\eta_1 \tanh(\eta_1 h) + \epsilon_2 \xi_1}{\epsilon_2 \xi_1 \tanh(\eta_1 h) + \eta_1} \tag{12}$$

Again

$$k_{z1}^2 = \bar{\epsilon}_1 k_o^2 - k_{y1}^2 = \bar{\epsilon}_2 k_o^2 + \eta_1^2 = k_o^2 + \xi_1^2 \tag{13}$$

and we define the effective dielectric constant for this structure as

$$\epsilon_{e1} = \bar{\epsilon}_1 - \left(\frac{k_{y1}}{k_o}\right)^2 \tag{14}$$

Note, however, that in equations (12) through (14) k_{z1}, k_{y1}, η_1, ξ_1 and $\bar{\epsilon}_1$ are complex quantities.

However, as a consequence of (1b), the imaginary parts of all quantities are much smaller than the corresponding real parts. Writing

$$k_{z1} = k_z' + jk_z'' \tag{15a}$$

$$k_{y1} = k_{y1}' + jk_{y1}'' \tag{15b}$$

$$\eta_1 = \eta_1' + j\eta_1'' \tag{15c}$$

$$\xi_1 = \xi_1' + j\xi_1'' \tag{15d}$$

$$\bar{\epsilon}_1 = \epsilon_1' + j\epsilon_1'' \tag{15e}$$

we take a Taylors series expansion of both sides of equation (12) about $(k_y' \quad \eta_1', \xi_1', \epsilon_1')$. Ignoring second order and higher order terms and equating real and imaginary parts, we get

$$k_{y1}' \tan(k_{y1}' d) = \eta_1' \frac{\epsilon_1'}{\epsilon_2} \frac{\eta_1' \tanh(\eta_1' h) + \epsilon_2 \xi_1'}{\epsilon_2 \xi_1' \tanh(\eta_1' h) + \eta_1'} \tag{16}$$

and

$$k_{y1}''[\sin(k_{y1}' d) + k_{y1}' d \cos(k_{y1}' d)] = \eta_1'[\epsilon_1'' \cos(k_{y1}' d)$$

$$- \epsilon_1' \sin(k_{y1}' d) \cdot k_{y1}'' d] \cdot \frac{N'}{D'} + \eta_1 \epsilon_1' \cos(k_{y1}' d) \cdot \frac{N'}{D'}$$

$$+ \eta_1' \epsilon_1' \cos(k_{y1}' d) \cdot \left(\frac{N''}{D'} - \frac{N'D''}{D'^2}\right) \tag{17}$$

where

$$N' = \eta_1' \tanh(\eta_1' h) + \epsilon_2 \xi_1' \tag{18a}$$

$$D' = \xi_1' \epsilon_2^2 \tanh(\eta_1' h) + \epsilon_2 \eta_1' \tag{18b}$$

$$N'' = \eta_1''[\tan h(\eta_1' h) + \eta_1' h \sec h^2(\eta_1' h)] + \epsilon_2 \xi_1'' \tag{18c}$$

$$D'' = \xi_1' \epsilon_2^2 \eta_1'' h \sec h^2(\eta_1' h) + \xi_1'' \epsilon_2^2 \tan h(\eta_1' h) + \eta_1'' \epsilon_2 \tag{18d}$$

The real and imaginary parts of (13) are:

$$\epsilon_1' k_o^2 - k_{y1}'^2 = \epsilon_2 k_o^2 + \eta_1'^2 = k_o^2 + \xi_1'^2 \tag{19}$$

$$\epsilon_1'' k_o^2 - 2k_{y1}' k_{y1}'' = 2\eta_1' \eta_1'' = 2\xi_1' \xi_1'' \tag{20}$$

Observe that (15) and (19) constitute three equations for the three unknowns k_{y1}', η_1', ξ_1'. Once these unknowns have been solved, their value can be substituted into (20) and (17). Note that equation (17) is a linear equation in k_{y1}'', as indeed, it should, since only the first term of the Taylor's series was kept. Ignoring higher order terms, equation (14) may be written as

$$\epsilon_{e1} = \epsilon_{e1}' + j\epsilon_{e1}'' = \epsilon_1' - \left(\frac{k_{y1}'}{k_o}\right)^2 + j\left(\epsilon_1'' - \frac{2k_{y1}' k_{y1}''}{k_o^2}\right) \tag{21}$$

Having defined the E.D.C. in equations (14) and (21) for the equivalent slab structure (Fig. 3c) we can now proceed solving for the wavenumbers in the x direction with a analysis similar to that in [3]. The tangential fields we are interested in matching now are E_y and H_z. From equations (4a) and (4c) we note

$$E_y \sim \phi^e \tag{22}$$

$$H_z \sim \frac{\partial \phi^e}{\partial x} \tag{23}$$

Writing ϕ^e as

$$\phi^e = \begin{cases} A \cos(u \frac{x}{a}) & 0 < x < a \\ B \exp[-\frac{w}{a}(x-a)] & x > a \end{cases} \tag{24}$$

we match the fields at x = a and obtain

$$A \cos(u) = B \tag{25}$$

$$-\frac{u}{a} A \sin(u) = -\frac{w}{a} B \tag{26}$$

from which one gets the eigenvalue equation

$$w = u \tan(u) \tag{27}$$

As before, by matching the fields along the z direction we also get another equation for u and w

$$k_2^2 = \epsilon_{e1} k_o^2 - \left(\frac{u}{a}\right)^2 = \epsilon_{e2} k_o^2 + \left(\frac{w}{a}\right)^2 \tag{28}$$

Notice that $u = u_r + ju_i$, $w = w_r + jw_i$ are in general complex numbers.

In the following sections three cases will be considered:

(i) $\mathrm{Re}\epsilon_{e1} = \epsilon_{e2}$, (ii) $\mathrm{Re}\epsilon_{e1} > \epsilon_{e2}$, and (iii) $\mathrm{Re}\epsilon_{e1} < \epsilon_{e2}$.

IV. RESULTS AND DISCUSSION

In Fig. (4) and Fig. (5) the solution for the equivalent dielectric constants defined in equations (14) and (21) are displayed for different values of ϵ_1' and ϵ_1. Since equations (12) and (16) are identical, Fig. (4) may be used to compute both ϵ_{e1}' and ϵ_{e2}. The equations were solved by iteration using Müller's Method, convergence was quite rapid and fairly insensitive to the starting point. The program is included in the appendix.

We now proceed to examine the first case (i.e., $\mathrm{Re}\epsilon_{e1} = \epsilon_{e2}$). First we note that from equation (28) we can solve for

$$w = \sqrt{\{a^2 k_o^2 [\epsilon_{e1} - \epsilon_{e2}] - u^2\}} \tag{29}$$

Since $\mathrm{Re}\,\epsilon_{e1} = \epsilon_{e2}$ equation (24) can be rewritten as

$$w = \sqrt{\{a^2 k_o^2 (\mathrm{Im}\Delta\epsilon_e) - u^2\}} \tag{30}$$

where $\Delta\epsilon_e = \epsilon_{e1} - \epsilon_{e2}$. Defining $v = a k_o \sqrt{\mathrm{Im}\Delta\epsilon_e}$, we see from equation (27) that all physical dependence of the transverse wave numbers can be defined in terms of a single variable $|v|$, called the normalized gain. Equation (27) is then solved, again using Müller's Method.

Figure (6) and (7) show the solutions for w_r and w_i vs. $|v|$. Figure (6), which indicates the rate of field decay in Region II, shows that gain (i.e., $\mathrm{Im}\Delta\epsilon_e > 0$) induced modes exist, and are in fact guided throughout. That is, the gain induced by the imaginary part of the effective dielectric constant is solely responsible for the field confinement. From figure (8) as well as from figure (9), which shows the percent of the cross-sectional

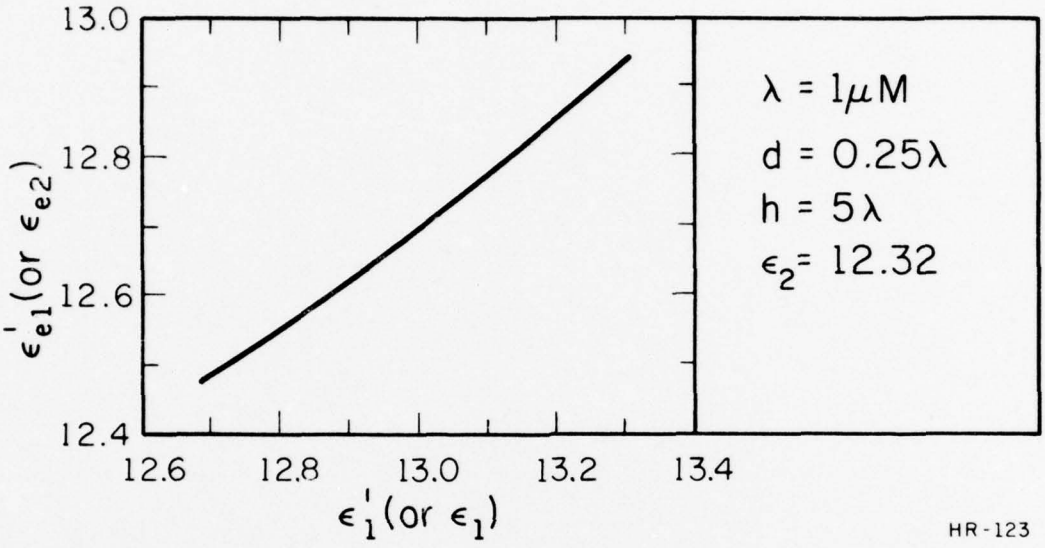

Fig. 4: Real part of the E.D.C. vs. the real part of the permittivity.

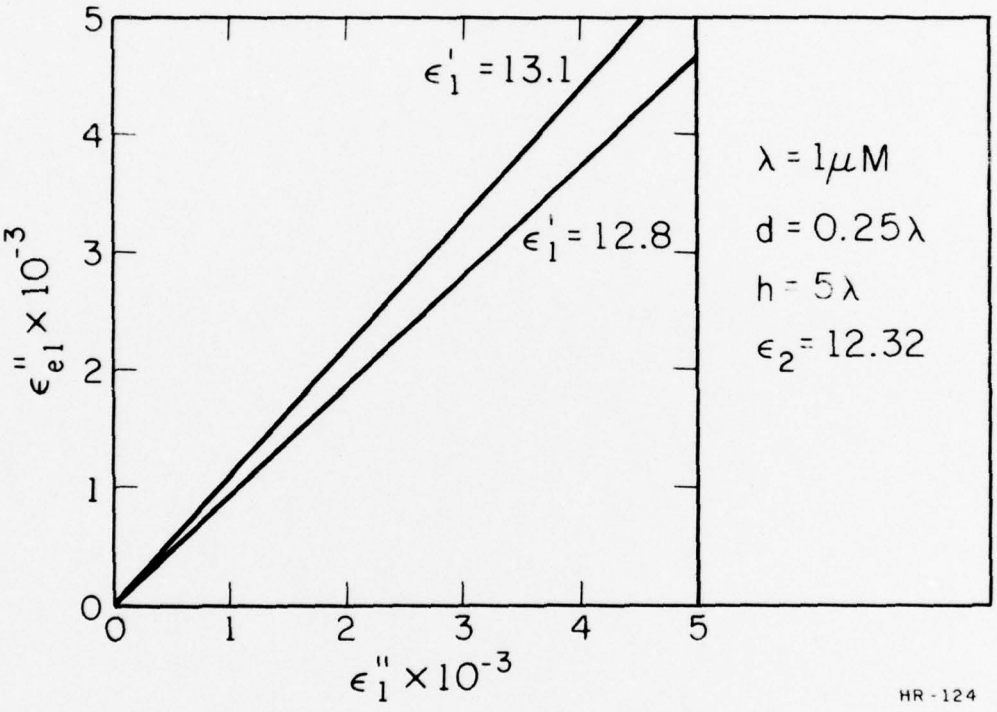

Fig. 5: Imaginary part of the E.D.C. vs. the gain.

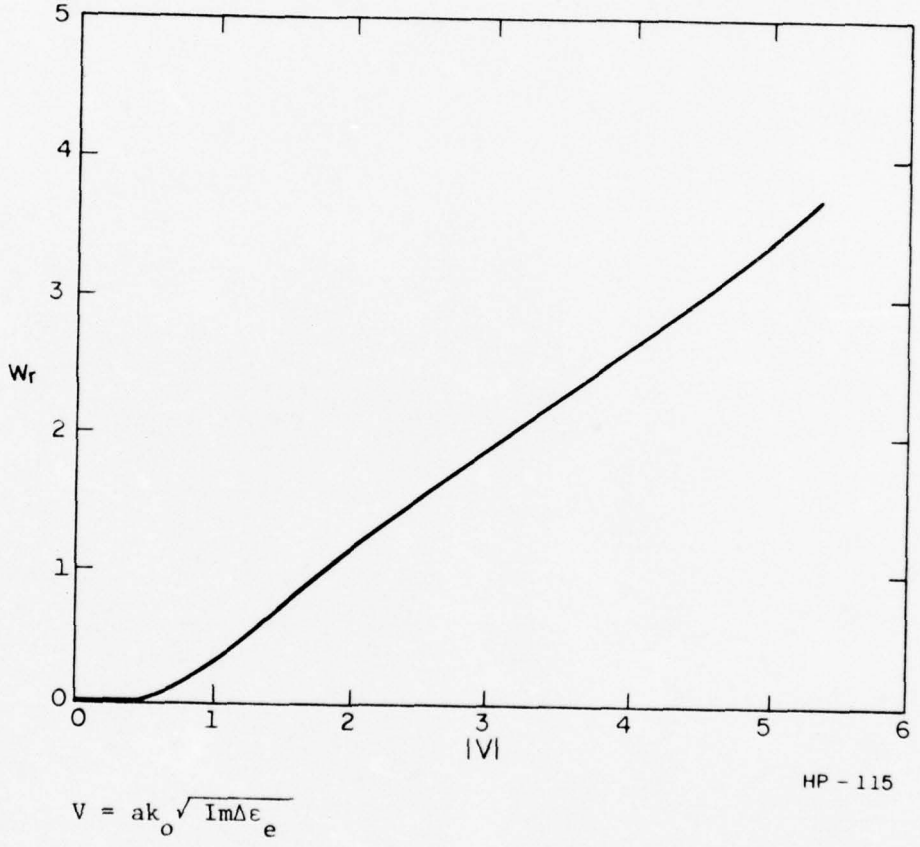

$$V = ak_o\sqrt{Im\Delta\varepsilon_e}$$

Fig. 6: Real part of W vs. $|V|$.

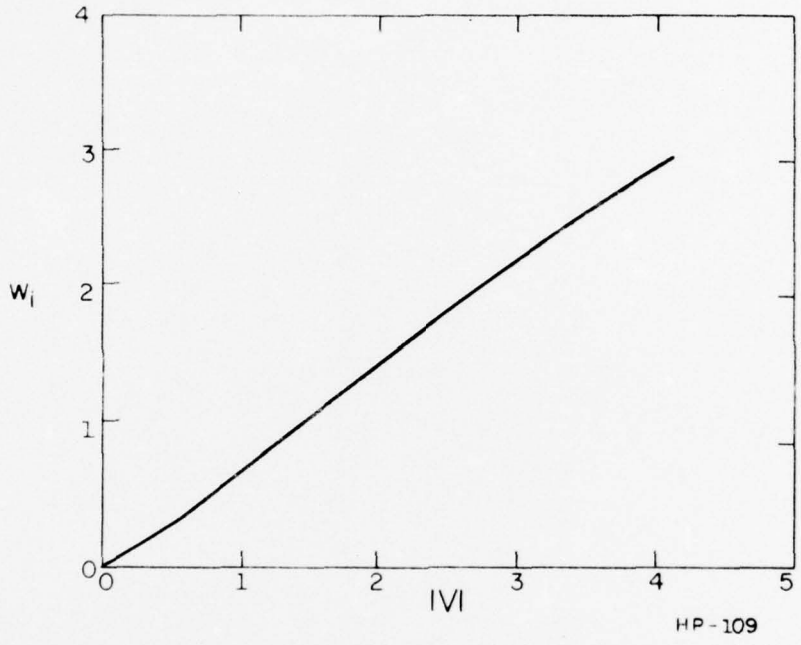

$$V = ak_o\sqrt{Im\Delta\varepsilon_e}$$

Fig. 7: Imaginary part of W vs. $|V|$.

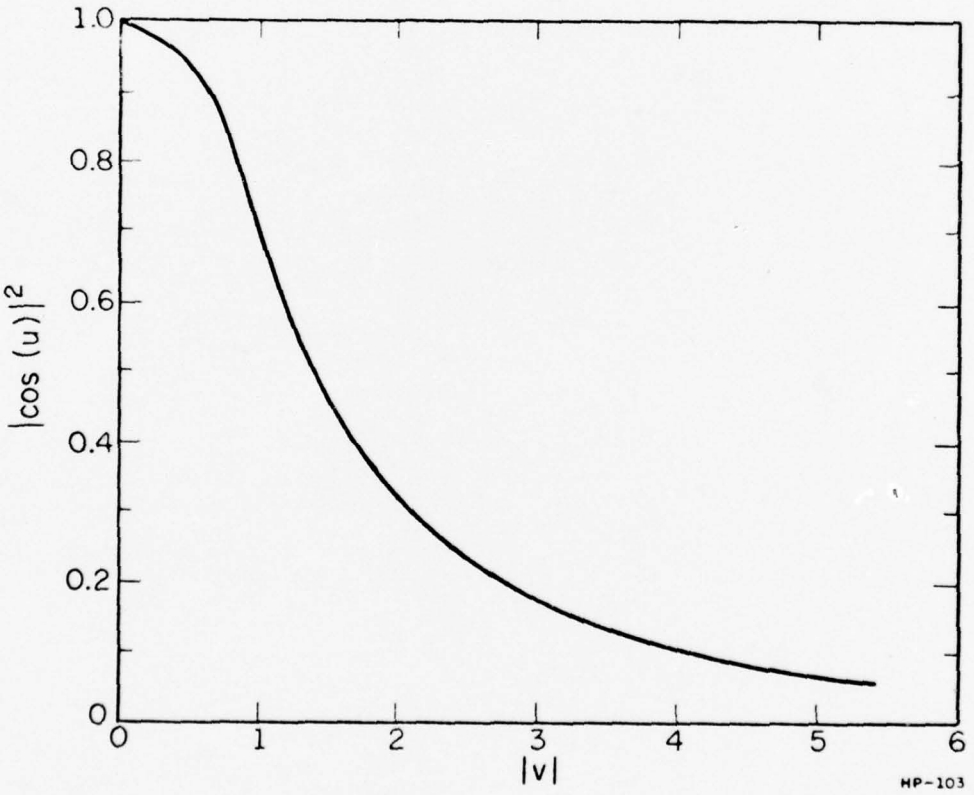

$V = ak_o\sqrt{Im\Delta\varepsilon_e}$

Fig. 8: Intensity of the field at x = a vs. $|v|$.

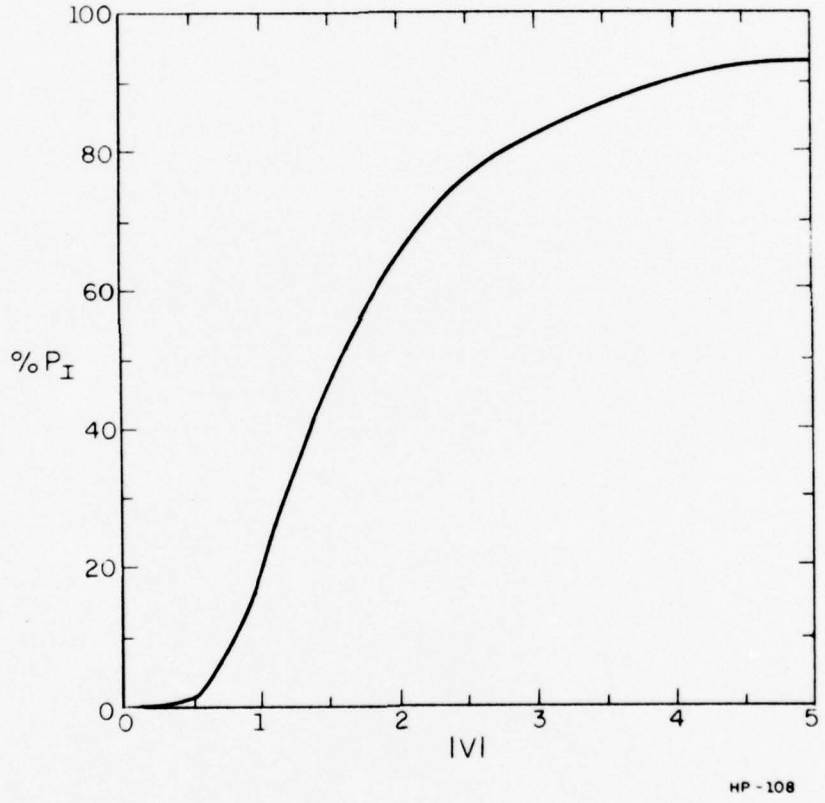

Fig. 9: Percent of power confined in Region I vs. $|V|$.

power in Region I, it is clear that the greater the gain, the more field is concentrated in Region I (active region). The values of the field intensity at x = a (Fig. 8) have been compared to the results obtained by Schlosser [3] and the agreement is good.

In Case (ii) the gain as well as the increase in the real part of the EDC in Region I contributes the confinement mechanism. However, this case will not be discussed further, because the confinement due to the real part is understood as the surface wave mechanism.

Case (iii) requires more careful examination. It is known that a quasi-mode (leaky wave mode) with low loss can exist in a passive channel waveguide, where the core material has lower refractive index than the surrounding medium, provided the core size is appreciably larger than the wavelength [6]. The latter is always the case in the configurations under study, as we have typically $\frac{2a}{\lambda} \approx 20$. As the epithet leaky suggest, propagation in such a "mode" is intrinsically accompanied by power loss due to leakage from the core into the surrounding medium. Hence, unless energy is continuously supplied as the wave propagates, the leaky mode will vanish below a detectable level after propagating over a finite distance.

In the present situation the supply mechanism is provided by gain in the region where wave is propagating. Hence, sufficient gain will sustain a stable cutoff mode, i.e., mode exhibiting no gain or attenuation outside the core. When this occurs, $w_r = 0$, as the field amplitude in Region II is expressed as $\exp[-w_r(\frac{x}{a} - 1)]$. We recall that the attenuation constant of a leaky mode is approximately inversely proportional to the index depression (see for instance, 1.6-34 of [6]). Hence, the cutoff

point is achieved with higher gain for decreasing refractive index depression, involving larger leakage.

For a given refractive index depression, as the gain increases above the value corresponding to cutoff (i.e., the amount of gain needed to compensate for leakage losses), then increasing field confinement takes place.

On the other hand, physical intuition suggests that field confinement is more sensitive to gain increases for smaller depressions. This is easily shown to be the case by means of the approximate analysis similar to that of [3]. We begin by again defining $v = a k_o \sqrt{\epsilon_{e1} - \epsilon_{e2}}$

$$v = a k_o \sqrt{\mathrm{Re}\Delta\epsilon_e} \left(1 - j \frac{\mathrm{Im}\Delta\epsilon_e}{|\mathrm{Re}\Delta\epsilon_e|}\right)^{\frac{1}{2}} \tag{31}$$

Since $\mathrm{Re}\Delta\epsilon_e < 0$

$$v = ja k_o \sqrt{|\mathrm{Re}\Delta\epsilon_e|} \left(1 - j \frac{\mathrm{Im}\Delta\epsilon_e}{|\mathrm{Re}\Delta\epsilon_e|}\right)^{\frac{1}{2}} \tag{32}$$

If $\dfrac{\mathrm{Im}\Delta\epsilon_e}{|\mathrm{Re}\Delta\epsilon_e|} \ll 1$, then

$$v \approx ja k_o \sqrt{|\mathrm{Re}\Delta\epsilon_e|} \left(1 - \frac{j}{2} \frac{\mathrm{Im}\Delta\epsilon_e}{|\mathrm{Re}\Delta\epsilon_e|}\right) \tag{33}$$

Let

$$v_i = a k_o \sqrt{|\mathrm{Re}\Delta\epsilon_e|} \tag{34}$$

$$v_r = a k_o \frac{\mathrm{Im}\Delta\epsilon_e}{2|\mathrm{Re}\Delta\epsilon_e|^{\frac{1}{2}}} \tag{35}$$

then

$$v = v_r + jv_i \tag{36}$$

In the case under study $\left|\frac{u}{v}\right|^2 \ll 1$, therefore,

$$w = v\sqrt{1 - \left(\frac{u}{V}\right)^2} \approx v$$

and

$$w_r = \frac{\pi a}{\lambda} \frac{\mathrm{Im}\Delta\epsilon_e}{|\mathrm{Re}\Delta\epsilon_e|^{\frac{1}{2}}} \tag{37}$$

and

$$\frac{dw_r}{d(\mathrm{Im}\Delta\epsilon_e)} \propto \frac{1}{|\mathrm{Re}\Delta\epsilon_e|^{\frac{1}{2}}} \tag{38}$$

In other words, the slope of w_r decreases for increasing depressions. The occurrence of the above two effects on the numerical solution is shown in figure (10). In particular, the approximate linearty of w_r with $\mathrm{Im}\Delta\epsilon_e$ implies the existence of a cross over point for two different values of $\mathrm{Re}\Delta\epsilon_e$. Figure (11) shows the solution for the imaginary part of w.

In figure (12) we show the field intensity at x = a, with $\mathrm{Im}\Delta\epsilon_e$ as the variable and $\mathrm{Re}\Delta\epsilon_e$ as the parameter. From figure (13), the numerical results indicate that for depressions less than .001 more gain is required to maintain guiding than for smaller depressions. However, for depressions larger than approximately .001 the pattern reverses: the greater the depression the less gain is required to insure guidance. This phenomena, just discussed above, can also be verified by a approximate solution of equation (27).

We start by assuming u_r is close to $\pi/2$.

$$u = \left(\frac{\pi}{2} + a\right) + jb \tag{39}$$

where $|a|$ and $|b| \ll 1$.

Since $\left|\frac{u}{v}\right|^2 \ll 1$.

$$w = v\left(1 - \left(\frac{u}{v}\right)^2\right)^{\frac{1}{2}} \approx v\left(1 - \frac{1}{2}\left(\frac{u}{v}\right)^2\right) \tag{40}$$

and (27) becomes

$$(v_r + jv_i)\left[1 - \frac{1}{2}\left(\frac{\frac{\pi}{2} + a + jb}{v_r + jv_i}\right)^2\right] = (\frac{\pi}{2} + a + jb)\tan(\frac{\pi}{2} + a + jb) \tag{41}$$

Since $v_r \ll 1$ and $v_i > 1$, v_r may be ignored. Furthermore, we note that $\tan(\frac{\pi}{2} + a + jb) \approx -1/(a + jb)$, and if $|\mathrm{Re}\Delta\epsilon_e|$ is large enough, such that $\left|\frac{1}{2}\left(\frac{\frac{\pi}{2} + a + jb}{j\,v_i}\right)^2\right| \ll 1$, equation (39) becomes:

$$j\,v_i = -\frac{(\frac{\pi}{2} + a + jb)}{a + jb} \tag{42}$$

Solving now for a and b we get

$$a = -\frac{\pi}{2}\left(\frac{1}{1 + v_i^2}\right) \tag{43}$$

$$b = \frac{\pi}{2}\left(\frac{v_i}{1 + v_i^2}\right) \tag{44}$$

To show the behavior at cutoff, we expand equation (28).

$$w_r^2 - w_i^2 + 2jw_rw_i = (a\,k_o)^2\mathrm{Re}\Delta\epsilon_e + j(a\,k_o)^2\,\mathrm{Im}\Delta\epsilon_e$$

$$- u_r^2 + u_i^2 - 2ju_ru_i \tag{45}$$

At cutoff, by definition, $w_r = 0$. It follows, then, that

$$(a\,k_o)^2\,\mathrm{Im}\Delta\epsilon_e = 2u_ru_i \tag{46}$$

Using the results from equations (41) and (42)

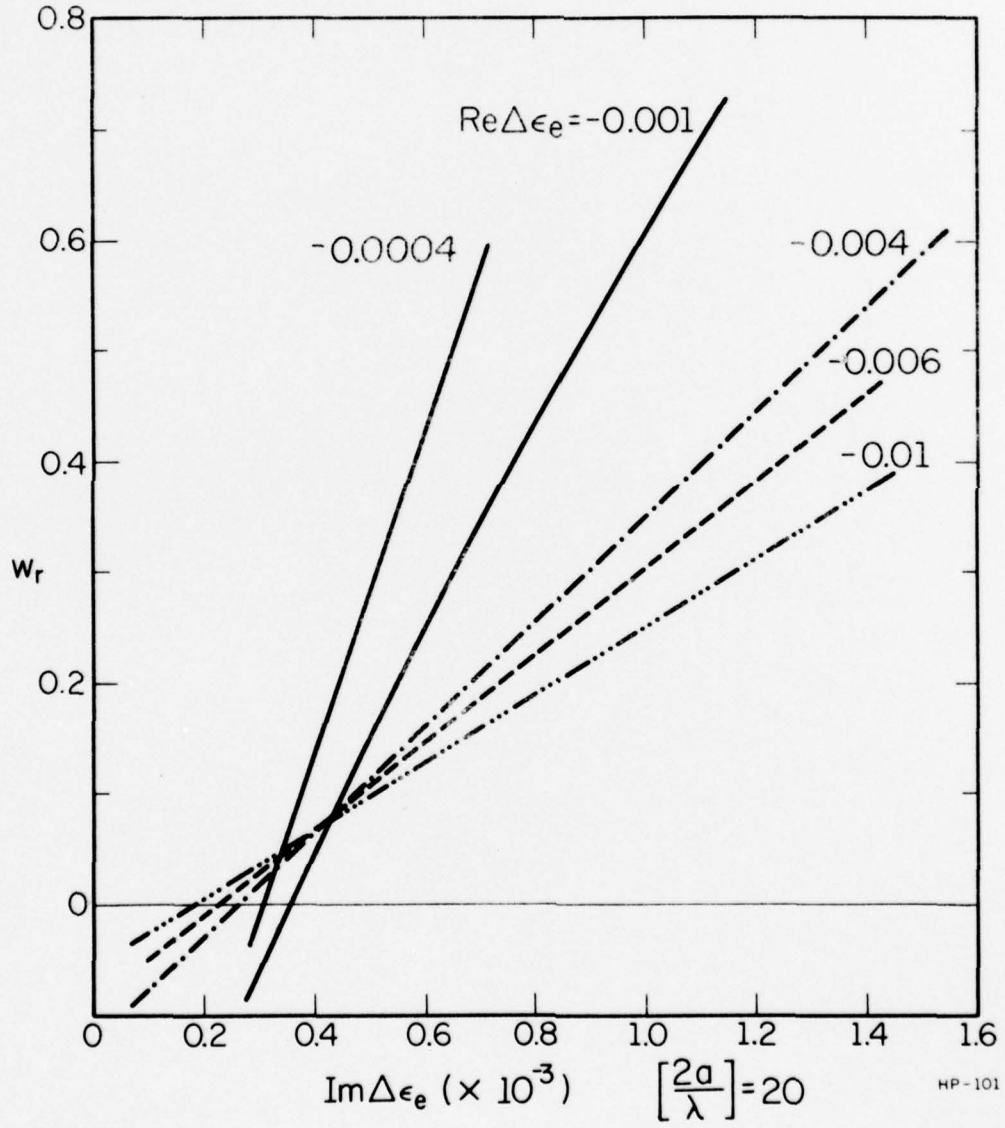

Fig. 10: Real part of W vs. $Im\Delta\epsilon_e$ with $Re\Delta\epsilon_e$ as parameter.

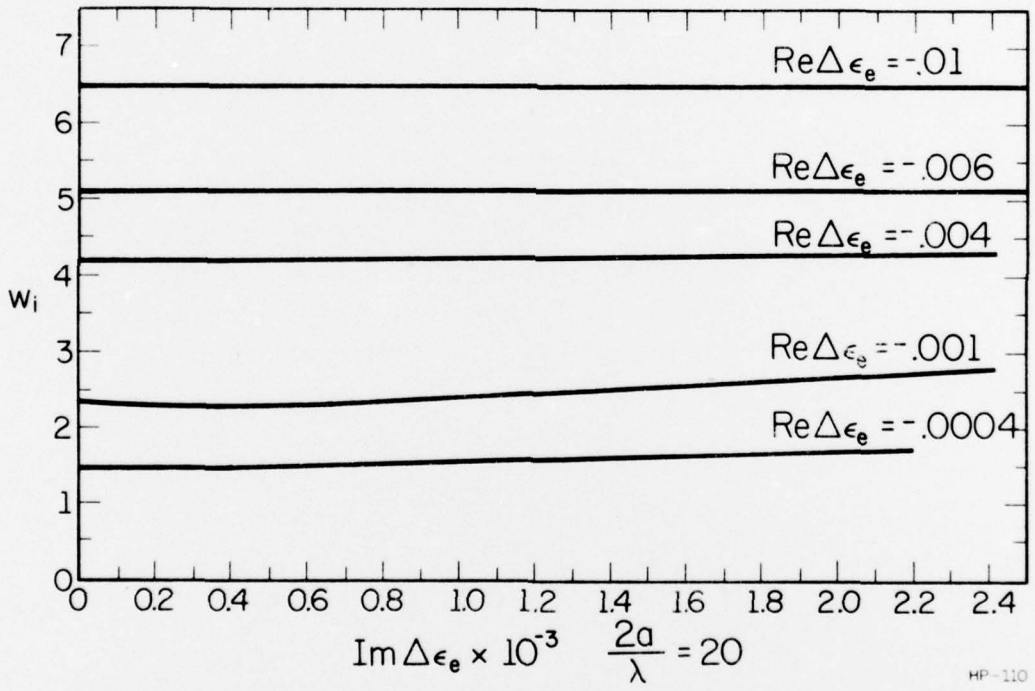

Fig. 11: Imaginary part of W vs. Im$\Delta\epsilon_e$ as parameter.

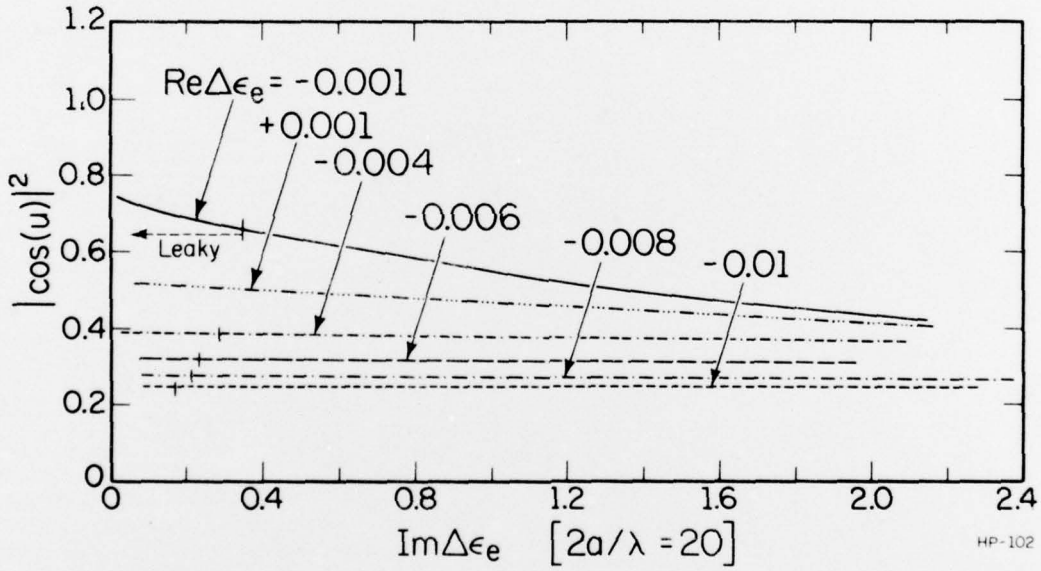

Fig. 12: Intensity of the field at x = a vs. $Im\Delta\epsilon_e$ with $Re\Delta\epsilon_e$ as parameter.

$$\mathrm{Im}\Delta\epsilon_e \text{ (at cutoff)} = \frac{1}{2}\left(\frac{\pi}{a\,k_o}\right)^2\left[\frac{v_i^3}{(1+v_i^2)^2}\right] \tag{47}$$

It can be immediately seen that, since $v_i > 1$,

$\mathrm{Im}\Delta\epsilon_e$ (at cutoff) $\propto \frac{1}{v_i} \propto 1/\sqrt{|\mathrm{Re}\Delta\epsilon_e|}$. That is, the larger the depression, the smaller the gain necessary to insure a guided mode. Equation (45) is plotted along side the numerical results in figure (13).

Looking at equation (32), it is possible to define a more general set of variables.

$$R = \frac{\mathrm{Im}\Delta\epsilon_e}{|\mathrm{Re}\Delta\epsilon_e|} \tag{48}$$

and

$$v' = \frac{2a}{\lambda}\sqrt{|\mathrm{Re}\Delta\epsilon_e|}\,. \tag{49}$$

Data, similar to that in figure (10) through (13), is presented in terms of these variables in figures (14) through (17).

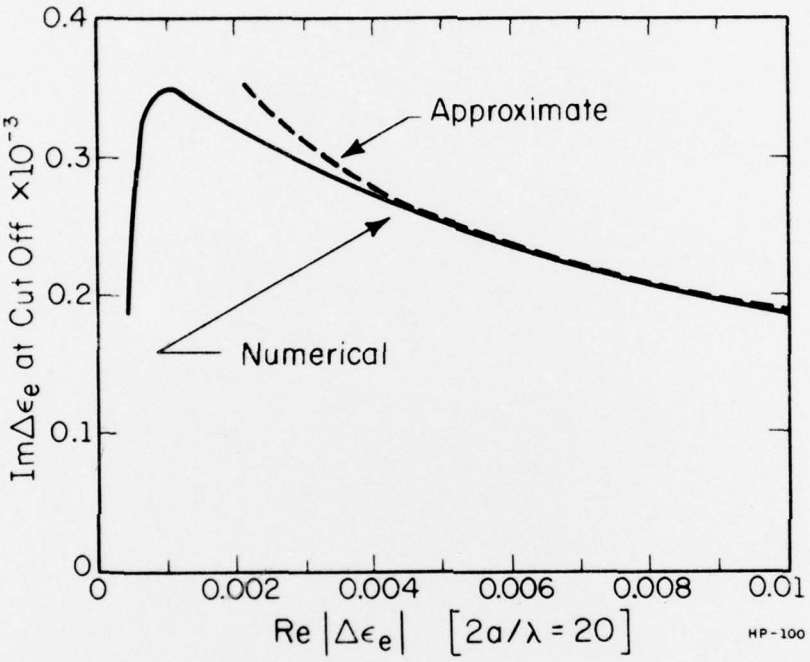

Fig. 13: $\mathrm{Im}\Delta\epsilon_e$ at cutoff vs. $\mathrm{Re}|\Delta\epsilon_e|$.

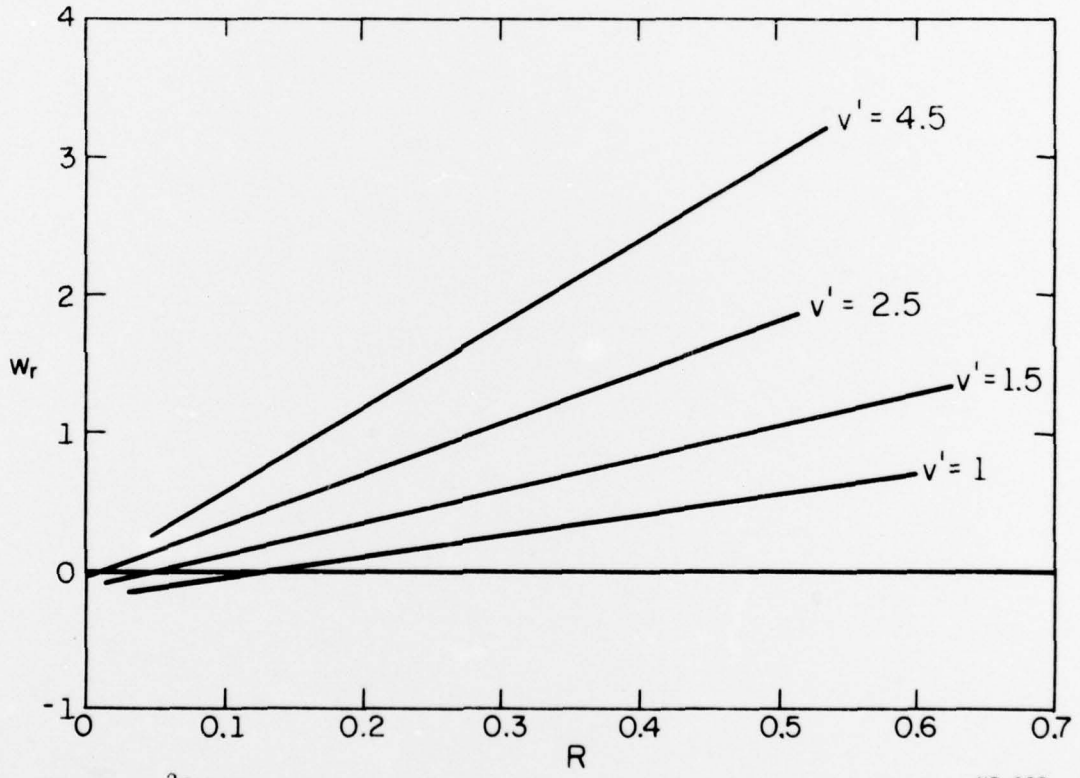

$$V' = \frac{2a}{\lambda}\sqrt{|Re\Delta\varepsilon_e|}$$

$$R = \frac{Im\Delta\varepsilon_e}{|Re\Delta\varepsilon_e|}$$

Fig. 14: Real part of W vs R with V' as parameter.

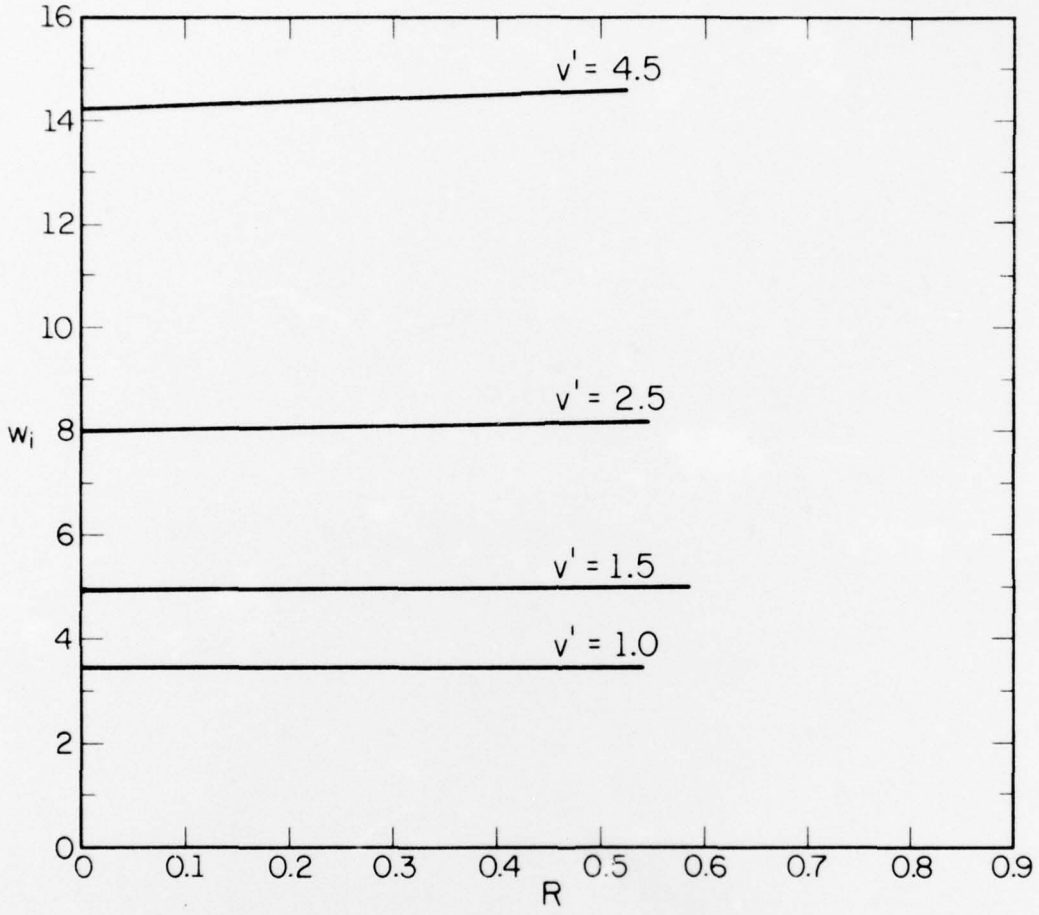

$$V' = \frac{2a}{\lambda}\sqrt{|Re\Delta\varepsilon_e|}$$

$$R = \frac{Im\Delta\varepsilon_e}{|Re\Delta\varepsilon_e|}$$

Fig. 15: Imaginary part of W vs. R with V' as parameter.

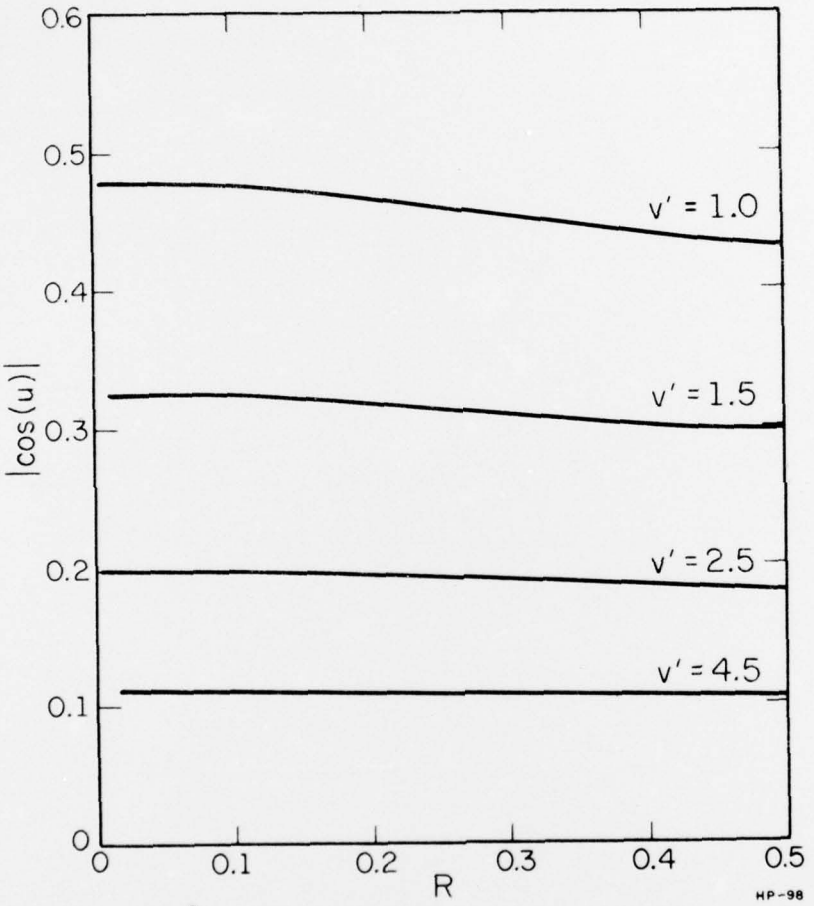

$$V' = \frac{2a}{\lambda}\sqrt{|Re\Delta\varepsilon_e|}$$

$$R = \frac{Im\Delta\varepsilon_e}{|Re\Delta\varepsilon_e|}$$

Fig. 16: Magnitude of the field at x = a vs. R with V' as parameter.

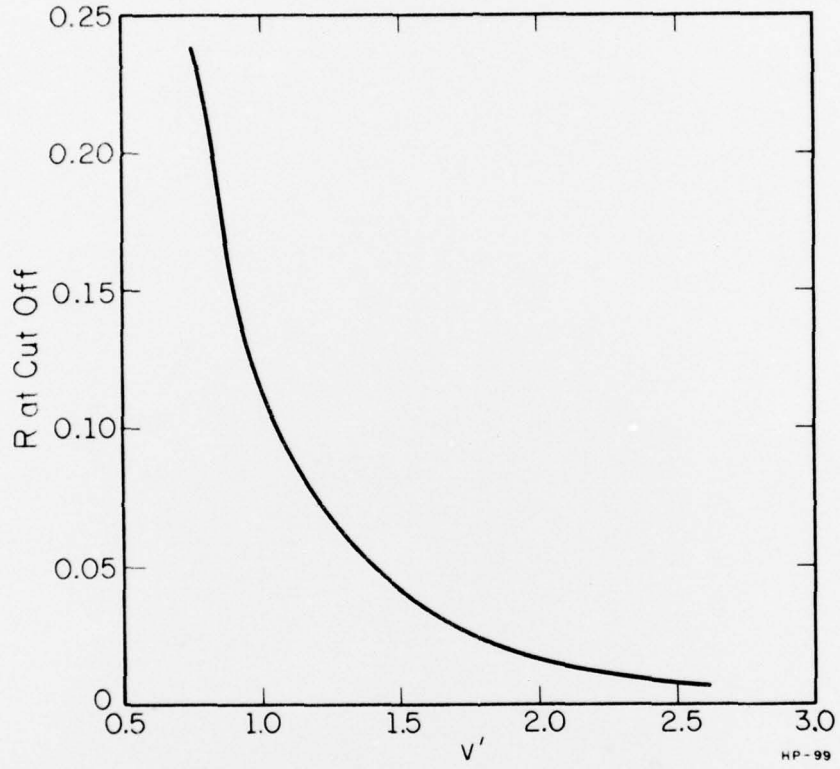

$$V' = \frac{2a}{\lambda}\sqrt{|Re\Delta\varepsilon_e|}$$

$$R = \frac{Im\Delta\varepsilon_e}{|Re\Delta\varepsilon_e|}$$

Fig. 17: R at cutoff vs. V'.

V. CONCLUSIONS

Two dimensional analysis, based on the concept of effective dielectric constant, was presented. Several numerical results are provided for the fundamental mode, illustrating gain induced confinement in the transverse direction. Gain induced modal confinement is shown possible even for a leaky wave structure and cutoff behavior is investigated.

VI. LIST OF REFERENCES

1. R. F. Harrington, Time-Harmonic Electromagnetic Fields, McGraw-Hill Book Company, Inc., New York, 1961.

2. A. Yariv, Quantum Electronics, John Wiley and Sons Inc., New York, 1975.

3. W. A. Schlosser, "Gain-Induced Modes in Planar Structures," Bell System Technical Journal, Vol. 52, No. 6, July-August 1973.

4. R. M. Knox and P. P. Toulios, "Integrated Circuits for the Millimeter Through Optical Frequency Range," Proceedings of the Symposium on Submillimeter Waves, N.Y., N.Y., March 31, April 1 & 2, 1970.

5. W. McLevige, T. Itoh and R. Mittra, "New Waveguides Structures for Millimeter-Wave and Optical Integrated Circuits," IEEE Trans. MTT-23, October 1975.

6. D. Marcuse, Theory of Dielectric Optical Waveguides, Academic Press, New York, 1974.

VII. APPENDIX

In this section a program to solve equations (16) and (17) is presented. The algorithm used was Muller's method. Convergence was quite rapid and fairly insensative to the starting point.

```
C       THIS PROGRAM SOLVES EQUATIONS (16) AND (17) USING MULLER'S
C       METHOD.ALL QUANTITIES ARE NORMALIZED WITH RESPECT TO
C       K0. WAVELENGTH(WAVEL),H,D,E2 MUST BE SUPPLIED. IMAX IS THE
C       MAXIMUM NUMBER OF ITERATIONS. A INITIAL GUESS Z3 MUST BE
C       SUPPLIED AS WELL AS THE EXPECTED ERROR (ERROR) OF THE
C       GUESS.
C       S1 INDICATES WHETHER ETA' IS REAL OF IMAGINARY.
C       EPS1 AND EPS2 ARE CRITERIA FOR STOPPING THE ITERATION


        COMMON E2,E1,H,D,WAVEL,PI,S1
        PI=3.1415
        E2=12.32
        PII=2.*PI
        WAVEL=1.E-6
        H=5.*WAVEL
        D=.25*WAVEL
C       NORMALIZE WITH RESPECT TO K0
        H=(PII/WAVEL)*H
        D=(PII/WAVEL)*D
        EPS1=1.E-5
        EPS2=1.E-9
        IMAX=50
        ERROR=.01
C       END OF DATA BLOCK


C       BEGIN ROOT FINDING ROUTINE
C       THE EQUATION WILL BE SOLVED FOR DIFFERENT VALUES OF E1
        DO 100 K=1,1
        E1=12.7-(K-1)*.01
        NC=NC+1
        NC2=0

C       INITIAL GUESS
        Z3=.481

        DELTA=ERROR
        IF(NC.GT.1) Z3=Z-.01
        Z1=Z3-DELTA
        Z2=Z3+DELTA
        VAL1=F(Z1)
        VAL2=F(Z2)
        VAL3=F(Z3)

 99     DEL1=(Z3-Z1)/(Z2-Z1)
        ALAM1=(Z3-Z2)/(Z2-Z1)
        G1=ALAM1**2*VAL1-DEL1**2*VAL2+(ALAM1+DEL1)*VAL3
        C1=ALAM1*(ALAM1*VAL1-DEL1*VAL2+VAL3)
        NC2=NC2+1
        S=1.
        IF(G1.LT.0) S=-1.
        ALAM=(-2.*DEL1*VAL3)/(G1+S*SQRT(ABS(G1**2-4.*DEL1*C1*VAL3)))
```

```
      V2=COS(ET*H)
      GO TO 32
30    V1=TANH(ET*H)
      V2=1.
32    TOP=S1*ET*V1+E2*XI(Z)*V2
      BTM=XI(Z)*E2*V1+ET*V2
      F=Z*SIN(Z*D)*BTM-ET*(E1/E2)*COS(Z*D)*(TOP)
      RETURN
      END


      FUNCTION ETA(Z)
      COMMON E2,E1,H,D,WAVEL,PI,S1
      S1=1.
C     IS ETA' IMAGINARY?
      IF(E1-E2-Z**2.LE.0) S1=-1.
      ETA=SQRT(ABS(E1-E2-Z**2))
      RETURN
      END


      FUNCTION XI(Z)
      COMMON E2,E1,H,D,WAVEL,PI,S1
      XI=SQRT(E1-1.-Z**2)
      RETURN
      END


      SUBROUTINE SS(Z,ET,AX)
      COMMON E2,E1,H,D,WAVEL,PI,S1
C     THIS SUBROUTINE COMPUTES KY''. SINCE AKY''=BE'' AND
C     FS=AKY''-BE'' (-B=RM), THIS IS A EQUATION IN TWO
C     UNKNOWNS. GIVEN FS1 (X1) AND FS2 (X2) FOR SOME VALUES
C     OF (KY'',E'') THE SLOPE IS COMPUTED.
C     FS=FS(KY',ETA',XI',KY'',E'')

      X1=FS(Z,ET,AX,1.E-3,1.E-3)
      X2=FS(Z,ET,AX,-1.E-3,1.E-3)
      RM=(X1+X2)/2.E-3
      A=(X1-1.E-3*RM)/1.E-3
      SLOPE1=-RM/A
C     NOW COMPUTE THE SLOPE FOR E(EQUIVALENT)'' .VS. E''
      SLOPE2=1.-Z*SLOPE1

      TYPE 50,E1,Z,SLOPE1,SLOPE2
50    FORMAT(' ',3HE1=,G11.4,2X,4HKY'=,G11.4,2X,7HSLOPE1=,
     1G11.4,2X,7HSLOPE2=,G11.4)
      RETURN
      END


      FUNCTION FS(B1,B2,B3,B4,B5)
C     B1=KY',B2=ETA',B3=XI',B4=KY'',B5=E''
      COMMON E2,E1,H,D,WAVEL,PI,S1
      D1=B2P(B1,B2,B4,B5)
      D2=B3P(B1,B3,B4,B5)
C     B2P=ETA'',B3P=XI''
      T1P=B2*TANH(B2*H)+E2*B3
      D1P=B3*E2**2*TANH(B2*H)+E2*B2
      T2P=D1*(TANH(B2*H)+B2*H*((1./COSH(B2*H))**2))+E2*D2
```

```
      Z=Z3+ALAM*(Z3-Z2)
      VAL4=F(Z)
      CRIT=ABS((Z-Z3)/Z3)

      IF (ABS(VAL4).LE.EPS1.OR.CRIT.LE.EPS2) GO TO 98
C     CONVERGENCE OBTAINED


      IF (NC2.GT.IMAX) GO TO 97
C     IF CONVERGENCE FAILS GO TO 97. IF NEITHER OF THE ABOVE
C     CONDITIONS ARE SATISFIED ,OBTAIN NEW POINTS AND GO BACK (99)
      Z1=Z2
      Z2=Z3
      Z3=Z
      VAL1=VAL2
      VAL2=VAL3
      VAL3=VAL4
      GO TO 99


C     CONVERGENCE HAS FAILED,TYPE OUT MESSAGE AND TERMINATE (101)
 97   TYPE 10
 10   FORMAT(' ','ITERATION OVER LIMIT')
      TYPE 11,VAL4,CRIT
 11   FORMAT(' ',5HVAL4=,G11.4,3X,5HCRIT=,G11.4)
      TYPE 12,Z,Z3,Z2,Z1
 12   FORMAT(' ',2HZ=,G14.7,2X,3HZ3=,G14.7,2X,3HZ2=,G14.7,2X,
     13HZ1=,G14.7)
      GO TO 101

C     CONVERGENCE OBTAINED. COMPUTE KY''
 98   TYPE 13,VAL4,CRIT
 13   FORMAT(' ',5HVAL4=,G11.4,3X,5HCRIT=,G11.4)
      TYPE 14,NC2
 14   FORMAT(' ',10HITERATION=,I4)
      ET=ETA(Z)
      AX=XI(Z)
      TYPE 15,Z,S1,ET,AX
 15   FORMAT(' ',3HKY=,G14.7,3X,G9.2,2X,4HETA=,G14.7,2X,
     13HXI=,G14.7)
C     INSERT PLOTTING BLOCK AND OTHER OUTPUT STATEMENT.
C     COMPUTE EFFECTIVE DIELECTRIC CONSTANT
      EQ=E1-Z**2
      TYPE 16,E1,EQ
 16   FORMAT(' ',3HE1=,G12.5,3X,3HEQ=,G12.5)
      CALL SS(Z,ET,AX)
C     SOLVE FOR SLOPE OF KY''


 100  CONTINUE
 101  STOP
      END


      FUNCTION F(Z)
      COMMON E2,E1,H,D,WAVEL,PI,S1
      ET=ETA(Z)
C     IF ETA' IS IMAGINARY COSH BECOMES COS ETC..
      IF(S1) 31,31,30
 31   V1=SIN(ET*H)
```

```
D2P=B3*E2**2+D1*H*((1./COSH(B2*H))**2)+D2*E2**2
1*TANH(B2*H)+D1*E2
F5=F4*(SIN(B1*D)+B1*D*COS(B1*D))-B2*(B5*COS(B1*D)
1-E1*SIN(B1*D)*B5*D)*(T1P/D1P)-D1*E1*COS(B1*D)*
1(T1P/D1P)-B2*E1*COS(B1*D)*((T2P/D1P)-(T1P*D2P)
1/(D1P**2))
RETURN
END


FUNCTION B2P(B1,B2,B4,B5)
COMMON E2,E1,H,D,WAVEL,PI,S1
B2P=(B5-2.*B1*B4)/(2.*B2)
RETURN
END


FUNCTION B3P(B1,B3,B4,B5)
COMMON E2,E1,H,D,WAVEL,PI,S1
B3P=(B5-2.*B1*B4)/(2.*B3)
RETURN
END
```

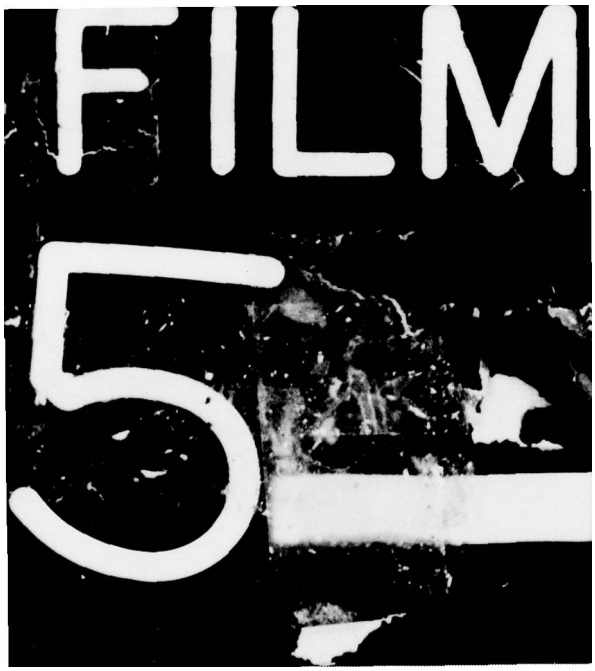
FILM
5